

# The Circumnuclear Star-forming Activities along the Hubble Sequence

Lei Shi, Qiusheng Gu and Zhixin Peng

Department of Astronomy, Nanjing University, Nanjing 210093, China  
e-mail: shileiaastro@yahoo.com; qsgu@nju.edu.cn

Received —; accepted —

**Abstract.** In order to study the circumnuclear star-forming activity along the Hubble sequence, we cross-correlate the Sloan Digital Sky Survey Data Release 2 (SDSS DR2) with the Third Reference Catalog of Bright Galaxies (RC3) to derive a large sample of 1015 galaxies with both morphological and spectral information. Among these, 385 sources are classified as star-forming galaxies and the SDSS fibre covered the circumnuclear regions (0.2 – 2.0 kpc). By using the spectral synthesis method to remove the contribution from the underlying old stellar population, we measure the emission lines fluxes accurately which are then used to estimate the star formation rates (SFRs). Our main findings are that: (1) Early-type spirals show much larger H $\alpha$  luminosities and hence higher SFRs, they also suffer more extinctions than late-type ones. The equivalent widths (EWs) of H $\alpha$  emission lines show the similar trend, however, the very late types (Sdm  $\sim$  Irr) do have large fractions of high EWs. (2) We confirm that  $D_n(4000)$  has strong correlation with the strengths of metallic absorption lines (such as CN band, G band and Mg Ib). Both these lines and the Balmer absorption lines show interesting variations between Sbc to Sd type galaxies. (3) The bar structure tightly relates with the enhanced star formation activity, this effect is even more significant in the early-type spirals. But we should note that the bar structure is not a necessary or sufficient condition for galaxies to harbor circumnuclear star formations.

**Key words.** galaxies: general - galaxies: stellar content - galaxies: statistics

## 1. Introduction

The star formation history is one of the most important problems for understanding the evolutions of the galaxies and also the universe. Enormous progress have been made during the last two decades. More precise diagnostics of global star formation rates (SFRs) have been obtained in a broad range of techniques: e.g., integrated optical emission line fluxes (Kennicutt 1983; Kennicutt et al. 1994; Madau et al. 1998), near-ultraviolet continuum fluxes (Donas & Deharveng 1984; Deharveng et al. 1994; Madau et al. 1998; Bell & Kennicutt 2001), infrared continuum fluxes (Harper & Low 1973; Rieke & Lebofsky 1978, Telesco & Harper 1980; Kennicutt et al. 1987), and radio emissions (Condon 1992; Cram et al. 1998). Kennicutt (1998) has presented an excellent review on star formation along the Hubble sequence.

A galaxy's morphology carries an important information for the study of star formation history in galaxies (e.g., Kennicutt 1998). Hubble sequence (Hubble 1926), as one of the most widely used classification of galaxies, is closely connected with the global star formation activities of galaxies. The basic view of global SFRs along the Hubble sequence shows that the equivalent widths (EWs)

of H $\alpha$  emission lines increase from virtually zero in E/S0 galaxies to about a couple of hundreds Å in late-type spiral and irregular galaxies (Kennicutt & Kent 1983; Kennicutt 1998). However, recent studies of H $\alpha$  imaging indicate that a significant fraction of the early-type spirals shows remarkable star formation activities (Young et al. 1996; James et al. 2004; Hameed & Devereux 2005).

Many galaxies are shown to harbor luminous star forming activities at the circumnuclear region with properties different from those of extended disks (Morgan 1958, Sérsic & Pastoriza 1967). Comprehensive surveys of the star formation properties of galactic nuclei have been carried out both in the optical band (Stauffer 1982, Keel 1983, Kennicutt et al. 1989, Ho et al. 1997a, b) and mid-IR photometry (Rieke & Lebofsky 1978, Scoville et al. 1983, Devereux et al. 1987, Giuricin et al. 1994). Ho et al. (1997a) found that the fraction of nuclear emission spectra with HII region-like line ratios increased from virtually zero in elliptical galaxies, 8% in S0 galaxies to 80% in Sc-Im galaxies. However, these could be contaminated by LINER or Seyfert nuclei.

In most galaxies, the nuclear SFRs are quite modest, while the highest SFRs are mainly seen in the IR observations because the very luminous starbursts are mostly as-

sociated with dense molecular gas and suffered substantial extinctions in the optical band. The details of these IR luminous circumnuclear properties could be seen in Veilleux et al. (1995), Lutz et al. (1996), and also in Kennicutt (1998).

In this paper, we cross-correlate the largest spectral database available from the Sloan Digital Sky Survey (SDSS) and the Third Reference Catalog of Bright Galaxies (RC3) to derive a large sample of galaxies with both morphological and spectral information, we thus are able to statistically study the star forming activities along the Hubble sequence. This paper is organized as follows: we will describe the sample selection and also give a brief introduction of the stellar synthesis model in Section 2; the statistical results are presented in Section 3; in Section 4, we will discuss bar influence on the star formation activities; finally, we present our main conclusions in Section 5.

## 2. Sample

The Sloan Digital Sky Survey (SDSS, York et al. 2000; Stoughton et al. 2002; Abazajian et al. 2003) is one of the most ambitious surveys, which aims to obtain nearly  $10^6$  galaxies and  $10^5$  quasars when completed. This provides us a great opportunity to explore the relations between the star-forming properties and their morphologies. We thus cross-correlate the SDSS galaxies (Data Release 2, Abazajian et al. 2004) with the RC3 catalog using the position-matching accuracy of 1 arc minute for most galaxies and 3 arcminutes for those without enough accurate positions in RC3 (see the introduction of RC3). We derived 983 galaxies with an average of positional differences of  $0.0749 \pm 0.052$  arc min, 11 galaxies with  $0.7246 \pm 0.1716$  arc min, and 33 galaxies with  $2.055 \pm 0.9156$  arc min. For those 44 galaxies with large positional differences, we checked one by one by using Sloan Digital Sky Survey/SkyServer<sup>1</sup>. Finally, we excluded 12 galaxies for confusion and derived a sample of 1015 galaxies, 39 of which were defined as AGNs in Véron-Cetty & Veron (2003) and excluded for further analysis. We derived consistent results by comparing with NYU Value-Added Galaxy Catalog (Blanton et al. 2005)<sup>2</sup>, where they have presented SDSS galaxies catalogue with RC3 information.

Since the SDSS spectrophotometry used the size-fixed fibre (3 arcseconds), according to the the physical covering size of the SDSS fibre, we divided the whole sample into three sub-samples which mainly depends on the SDSS fibre covering region size: (1) 33 nuclear sub-sample, the fiber covering the region of less than 200 pc; (2) 824 circumnuclear sub-sample, where the fiber covers region of 0.2 kpc  $\sim$  2 kpc; (3) 119 disk sub-sample, covering the region larger than 2 kpc. Just like most, if not all, our sample will suffer from the Malmquist bias. In the following we will only concentrate on the circumnu-

clear sub-sample, with the relatively narrow redshift range of [0.00344,0.0344], and we will also use the distance-independent parameters (such as EWs and H $\alpha$  luminosity normalized by the fibre covering size) as indicators of SFRs, both of which will reduce the Malmquist effect for this study.

Though RC3 (de Vaucouleurs et al. 1991) has been widely used in astrophysical researches, many excellent works have been carried out both in photometric and spectroscopic observations ever since then, which undoubtedly revised some galaxies' morphological classifications (such as de Souza, Gadotti & dos Anjos 2004). As the NASA Extragalactic Database (NED) morphological types are the most up-to-date types in existence, we will use the NED morphologies for this work.

The results of cross-correlation between RC3 and SDSS DR2 of all the 976 galaxies are shown in Table 4, which contains the galaxy name (Column 1); R.A. and Dec. (2000, Column 2-3); redshift (Column 4); stellar and nebular extinctions (Column 5-6); luminosity of far-IR, in unit of log erg s<sup>-1</sup> (Column 7); morphology from NED (Column 8).

**Table 1.** The frequencies with different morphological types for the circumnuclear sample

Galaxy Type	E	L	S	Irr	Uncertain	Total
Number	43	127	536	18	100	824
Percentage	5.2	15.4	65.0	2.2	12.1	100

All galaxies were obtained from the cross-certification of RC3 and SDSS DR2 with the redshifts ranging from 0.0034 to 0.0344. The types are taken from NED calculated by using the definition of de Vaucouleurs et al. (1991).

Here we have combined all the elliptical galaxies into index T = -2, and included peculiar ones to Irregular galaxies (T = 10) for simply assuming that they may all involved in various merger processes. The index T = 13 are set for the uncertain or unusual type galaxies and will be excluded from the statistical studies. Table 1 gives the number of each main branches of Hubble sequences for the circumnuclear sample, which contains 43 ellipticals, 127 lenticulars, 536 spirals and 18 irregulars. Just like most, if not all, galaxy samples, the current circumnuclear sample of galaxies can not be considered complete. We hope that the much larger number of galaxies could reduce the problem of incompleteness.

In most normal galaxies, stellar light dominates the continuum and absorption lines at optical band. These absorption features can certainly contaminate the nebular emissions which will be useful for understanding the physical properties of galaxies. Moreover, the stellar spectrum alone may provide direct measurements on the stellar population, velocity dispersion and star formation his-

<sup>1</sup> <http://cas.sdss.org/astro/en/tools/search/>

<sup>2</sup> <http://wassup.physics.nyu.edu/vagc/>

tory (SFH) etc. Thus how to properly decompose the stellar component from the integrated spectrum becomes the first step to interpret the nuclear properties.

We use the same stellar population synthesis code provided by Roberto Cid Fernandes, called *starlight V2.0*, for spectra synthesis, which fits an observed spectrum  $O_\lambda$  with a linear combination of  $N_*$  simple theoretical stellar populations (SSP) computed with evolutionary synthesis models of Bruzual & Charlot (2003, BC03). The methodology of the code is described in detail by Cid Fernandes et al. (2004b). In this work we adopt a base with  $N_* = 45$  SSPs, with 3 metallicities:  $Z = 0.2, 1$  and  $2.5 Z_\odot$ , each of which has 15 ages ranged as 0.001, 0.003, 0.005, 0.01, 0.025, 0.04, 0.10, 0.29, 0.64, 0.90, 1.4, 2.5, 5.0, 11 and 13 Gyrs. The match between model and observed spectrum is evaluated by the ruler of  $\chi^2 = \sum_\lambda [(O_\lambda - M_\lambda) w_\lambda]^2$ , where  $w_\lambda^{-1}$  is the error in  $O_\lambda$ . The search for the best solution (also a minimum  $\chi^2$ ) is carried out by using a simulated annealing plus Metropolis scheme, consisting of a series of 6 likelihood-guided Metropolis explorations through the parameter space (see Cid Fernandes et al. 2001 for a detailed discussion of the Metropolis method applied to the population synthesis problem), which searches for the minimum  $\chi^2$ . Spectral regions around emission lines, bad pixels or sky residuals are masked out by setting  $w_\lambda = 0$ .

The spectra were first rebinned to 1 Å bins and redshift corrected to the rest-frame by the standard IRAF<sup>3</sup> procedures. Then we corrected the spectra for Galactic Extinction using the reddening law of Cardelli et al (1989) and the  $A_B$  values listed in NED (Schlegel, Finkbeiner & Davis 1998) before starting the synthesis. We normalize the SSP bases at  $\lambda_0 = 4020$  Å, while for the observed spectra we use the median value between 4010 and 4060 Å. Every spectrum has been synthesized from 3650 to 8000 Å.

Since in this paper we will only concentrate on the star forming galaxies, we use the criteria given by Kauffmann et al. (2003) to distinguish the potential AGNs or the composite ones from star-forming galaxies. Figure 1 is the diagram of Baldwin, Phillips, & Terlevich (1981, BPT) for our sample. After adopting the line of Kauffmann et al. (2003), we derived 385 star forming galaxies and 438 AGNs or the composite ones. There is still one galaxy not presented in this diagram, because it shows no emission line features both in its original spectrum and the continuum subtracted one. Figure 2 shows the morphological distribution for these star-forming galaxies.

### 3. Statistic Results

#### 3.1. The Emission Line Features

We have measured the emission line features from the "pure emission" spectra, which are derived by subtracting

<sup>3</sup> IRAF is distributed by the National Optical Astronomy Observatory, which is operated by the Association of Universities for Research in Astronomy, Inc., under cooperative agreement with the National Science Foundation

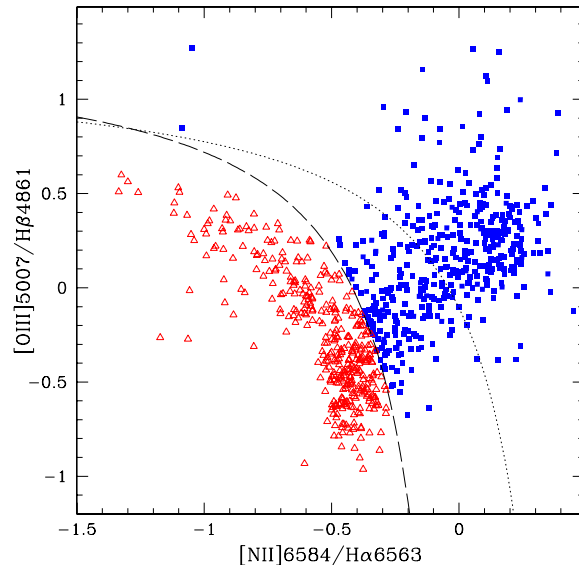


**Fig. 1.** The distribution of the galaxies in our circumnuclear sample in the BPT emission line ratio diagram. The dotted line is from Kewley et al. (2001), and the long-dashed line is from Kauffmann et al. (2003), which will be used in this paper as the criteria to distinguish star-forming galaxies and the AGNs or the composite ones. The filled rectangles show the AGNs or the composite ones; while the open triangles represent the star-forming galaxies.

synthetic spectrum from the observed one. The measurement is automatic and the windows for emission line and continuum are listed in Table 2.

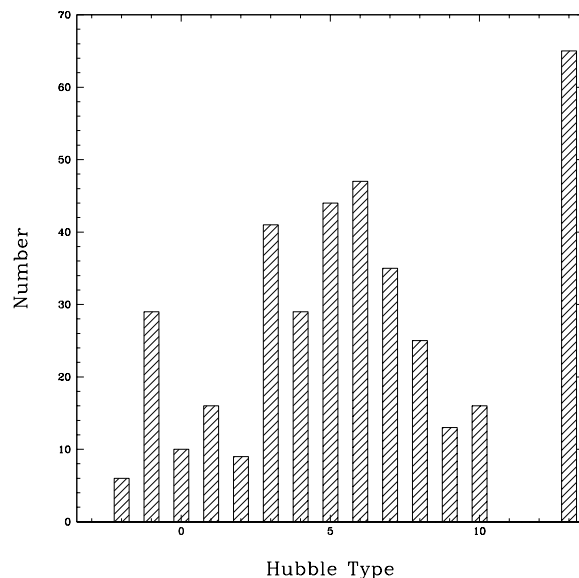


**Fig. 2.** The morphological distribution for the 385 star-forming galaxies. We set the T-index of those galaxies with uncertain types as  $T = 13$ .

**Table 2.** Definitions of emission line windows

Emission Lines	Windows	Continuum Windows
H $\delta$ 4101	4090-4114	4055-4065 4135-4145
H $\gamma$ 4340	4328-4352	4250-4260 4400-4410
HeII 4686	4672-4700	4655-4665 4720-4730
H $\beta$ 4861	4851-4871	4825-4835 4885-4895
[OIII] 4959	4949-4969	4915-4925 5035-5045
[OIII] 5007	4997-5017	4915-4925 5035-5045
H $\alpha$ 6563	6556-6573	6520-6530 6610-6620

All wavelengths are in units of  $\text{\AA}$ .

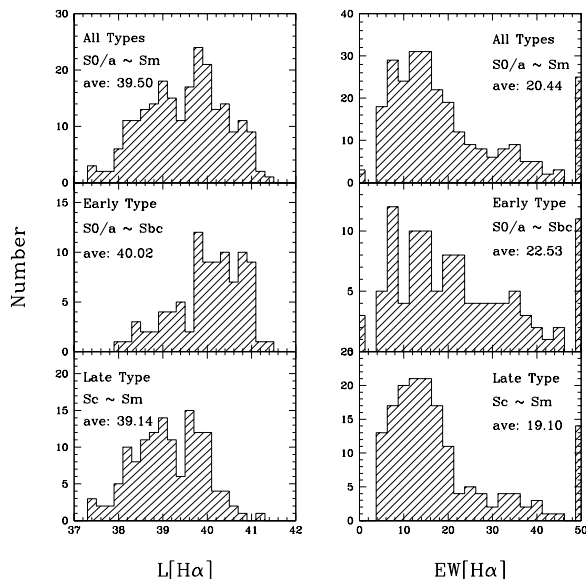


**Fig. 3.** The histogram of extinction-corrected  $L(H\alpha)$  and  $EW(H\alpha)$ . From the top to bottom are the distributions of  $H\alpha$  luminosities and equivalent widths for all, early-type and late-type galaxies. The luminosities have all been corrected for Balmer extinction.

The  $H\alpha$  luminosities of the sample span a large range, from about  $10^{37}$  to  $10^{42}$   $\text{erg s}^{-1}$  (Figure 3). The early-type (S0 – Sbc) spirals extend much larger toward the high end of  $L(H\alpha)$  than the late-type (Sc – Im) ones<sup>4</sup>, which is consistent with Ho et al. (1997a). The median value of  $\log(L[H\alpha])$  is 40.02 and 39.14 for the early-type and late-type galaxies respectively. We should note that this trend is truly exist and slightly exaggerated by the effect of nebular extinctions. Table 5 shows the flux densities of H $\beta$  4861 (Column 2), [OIII] 5007 (Column 3), [NII] 6548,6584 (Column 4-5), H $\alpha$  6563 (Column 6), and [SII] 6717,6731 (Column 7-8) for our sample, all in units of  $10^{-17} \text{erg s}^{-1} \text{cm}^{-2}$ . Corresponding equivalent widths are shown in Table 6 for all the sample galaxies, in units of  $\text{\AA}$ .

<sup>4</sup> From here to the end of this paper, the early-type refers to S0/a–Sbc and the late-type refers to Sc–Sm as the same in Ho et al. (1997a, b).

### 3.2. Extinction

The dust extinction can have considerable impact on the thermal balance of the interstellar medium and on the formation of  $H_2$  molecules, which have important consequences on the efficiency of star formation (Omukai 2000, Hirashita & Ferrar 2002). The nebular extinction is derived from the observed Balmer decrement ( $H\alpha/H\beta$ , see Torres-Peimbert, Peimbert & Fierro 1989). Assuming Case B recombination and a standard reddening law (Cardelli et al. 1989), we obtained the V-band extinction:

$$A_V^{nebular} = 6.31 \times \log \left( \frac{F_{H\alpha}/F_{H\beta}}{I_{H\alpha}/I_{H\beta}} \right), \quad (1)$$

where  $F_{H\alpha}/F_{H\beta}$  and  $I_{H\alpha}/I_{H\beta}$  are the observed and intrinsic flux ratios of H $\alpha$  and H $\beta$  respectively. Here we use the intrinsic ratio of  $I_{H\alpha}/I_{H\beta}$  to be 2.86 (Osterbrock 1989). Galaxies with either one of the two lines insufficient in fluxes (less than  $3\sigma$ ) were excluded here. We also derived some negative values of  $A_V$ . Since these were unexpected for the common model of extinction and may actually be overestimated (see Cid Fernandes et al. 2005 for the details), we set them as zero in studying the relation between the extinctions and Hubble types, and also in the previous study of H $\alpha$  luminosities.

It is believed that emission lines suffer more extinctions than stellar light (Calzetti, Kinney & Storchi-Bergmann 1994; Gordon et al. 1997; Mas-Hesse & Kunth 1999). More recently, Cid Fernandes et al. (2005) have applied the synthesis model on a large number of SDSS galaxies and get a linear bisector fitting  $A_V^{Balmer} = 0.24 + 1.81A_V$ . Since we use the same code as Cid Fernandes et al. (2005), it is not surprised that we get similar results.

Figure 4 shows the distribution of both the stellar and nebular extinctions ( $A_V$ ) along the Hubble sequence. We find that the nebular extinction decreases from early-type spirals to late-type spirals, which is consistent with Ho et al. (1997a) and Stasińska et al. (2004). while the trend of the stellar extinction is almost flat with slight variations among morphology types. This is accessible, since the stellar extinction represents the comparably old stars which are believed to have exposed from the surrounding molecular clouds.

### 3.3. Star Formation Rates

We have calculated the star formation rate from the extinction-corrected H $\alpha$  luminosity using Kennicutt’s (1998) conversion,

$$\text{SFR} (M_\odot \text{ yr}^{-1}) = 7.9 \times 10^{-42} L(H\alpha) (\text{ergs s}^{-1}), \quad (2)$$

Here we get an average SFRs of  $0.14 M_\odot \text{ yr}^{-1}$  with the median value of  $0.04 M_\odot \text{ yr}^{-1}$  for those with  $A_V$  or no sufficient fluxes in both H $\alpha$  and H $\beta$  lines which would be set as zero in SFRs of our 385 galaxies. These values are consistent with Ho et al. (1997a). Figure 5 (top) shows the distribution of star formation rates as a function of Hubble T-types. We find that the spiral galaxies of type Sb show the

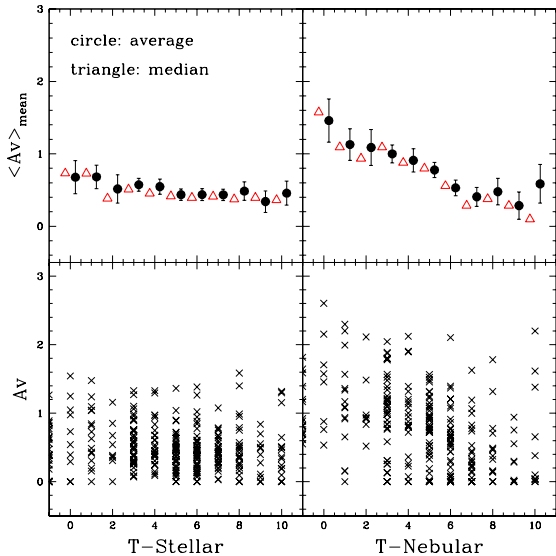


**Fig. 4.** The distribution of extinction along the Hubble sequence. The left two panels are the distributions of stellar extinctions (bottom panel) and their median (open triangles) and average values (filled circles). The error bar represents the deviation in the mean. The right plots are for the nebular extinctions.

highest star formation rate, which is slightly different from the global properties of the  $H\alpha$  survey (James et al 2004, peaking at Sbc and Sc). There exists a clear trend along the Hubble types with the values of  $SFR(H\alpha)$  decreasing from early-type spirals to the late-type ones (Figure 5, bottom). This is consistent with Stauffer (1982), Keel (1983) and Ho et al. (1997a). Many works have emphasized the aperture effect, here we just normalize the SFR by the corresponding aperture areas. This simple process will undoubtedly induce some bias, however, it is worth to see the general trend. Figure 6 shows the trend of SFRs per  $\text{kpc}^2$  along the Hubble sequence. Though it is a little bitter weaker, we still find that early-type spirals do show higher SFRs  $\text{kpc}^{-2}$  than the late-type spirals. Thus while luminous nuclear starbursts may exist in the entire range of spirals (Rieke & Lebofsky 1978; Devereux 1987), the relative effect is much stronger for the early-type spirals. We also calculated the SFRs from the far-Infrared emissions available in the RC3. Figure 7 shows the FIR-SFRs along the Hubble types. Again, we could find the early-type spirals do show higher SFRs but not significantly exceed those of late types.

The equivalent width of  $H\alpha$  ( $EW[H\alpha]$ ), which represents the efficiency of the star forming activity, shows the similar result (Figure 3). In Figure 8, we present the variations of EWs among each Hubble type. We find that early-type spirals show large equivalent widths (EWs), especially for those S0/a  $\sim$  Sab galaxies. From Sbc to Sd type, galaxies show similar EWs, and for the end of the sequence (Sdm  $\sim$  I) we see clearly a large fraction of high equivalent widths.

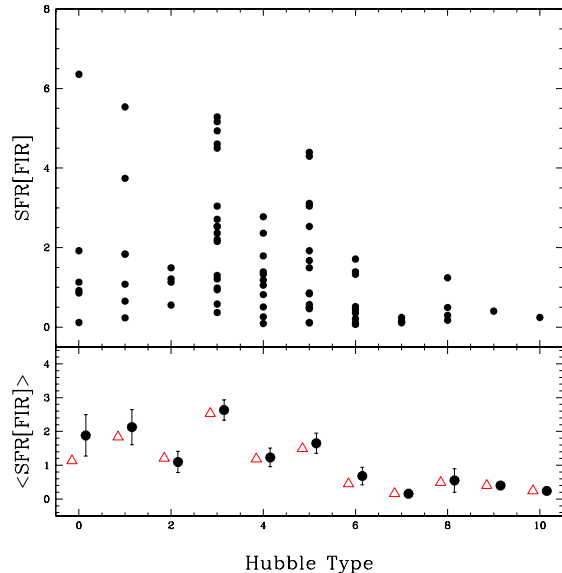


**Fig. 5.** The circumnuclear SFRs of  $H\alpha$  along the Hubble sequence. Most galaxies show moderate SFRs, while large dispersions are seen in early-type galaxies. The median SFR values show a clear trend decreasing from early-type to late-type spirals. Symbols are the same meaning as Figure 4

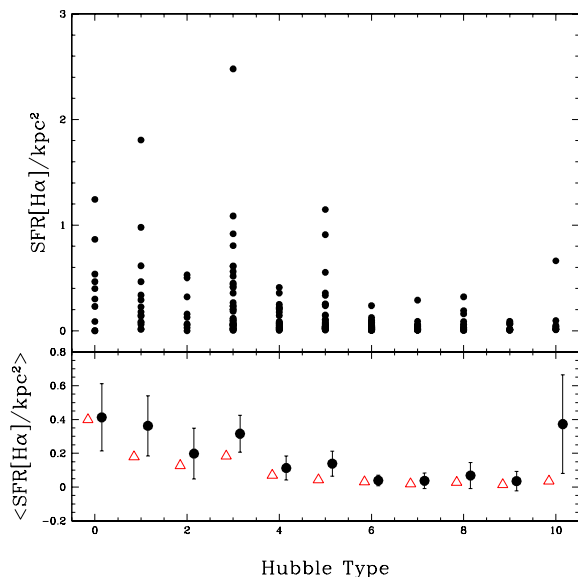


**Fig. 6.** The distribution of SFRs normalized by the aperture areas. The trend is much weaker, however, the early-type galaxies do show higher median values of  $SFR(H\alpha)$ .

For all Hubble types, the moderate values of both SFRs and EWs of  $H\alpha$  are very common in the distributions, however, large dispersion among the same type do exist, which is consistent with James et al. (2004). Furthermore, we also find some elliptical and lenticular galaxies show considerable high  $SFR(H\alpha)$  and  $EW(H\alpha)$ . Since  $H\alpha$  emis-

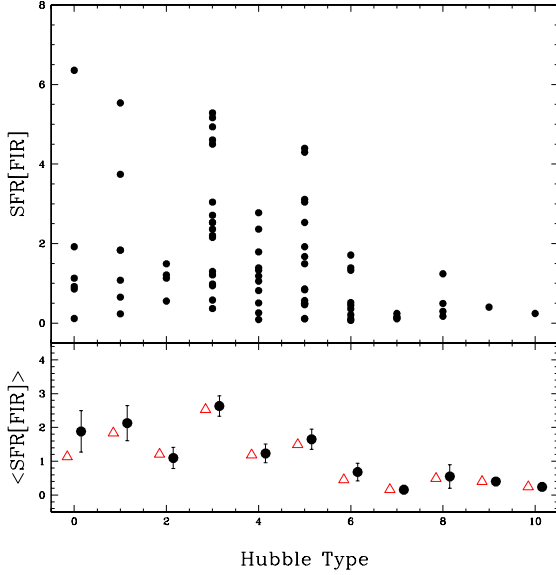


**Fig. 7.** The distribution of FIR SFRs among Hubble types. The early-type spirals show comparably larger values, however, this may due to the lack of data in late-type spirals. Symbols are the same meaning as Figure 4

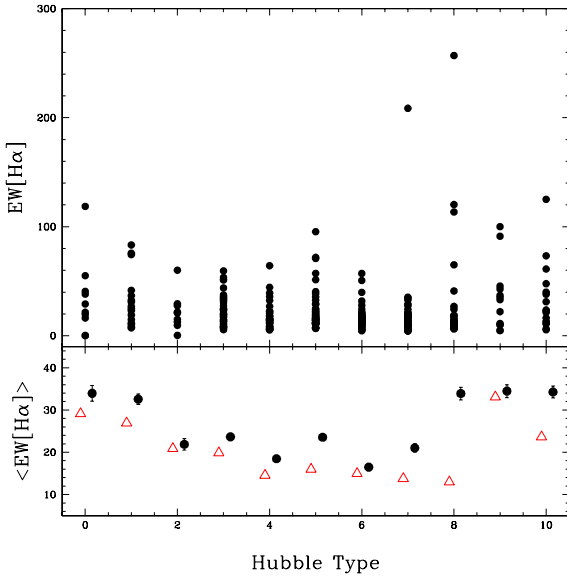


**Fig. 8.** The distribution of  $EW(H\alpha)$  among the Hubble types. There is no significant trend found with morphology types, however, the late-type galaxies do show comparably larger dispersions and higher median values. The triangles represent the median values and the filled circles are the averages, which may be affected by the few extremely larger ones.

tion has a different origin in ellipticals and S0's than in spiral galaxies, which is usually due to the nuclear activities or merger/peculiar interactions, we will not discuss these ellipticals and S0's in this paper.

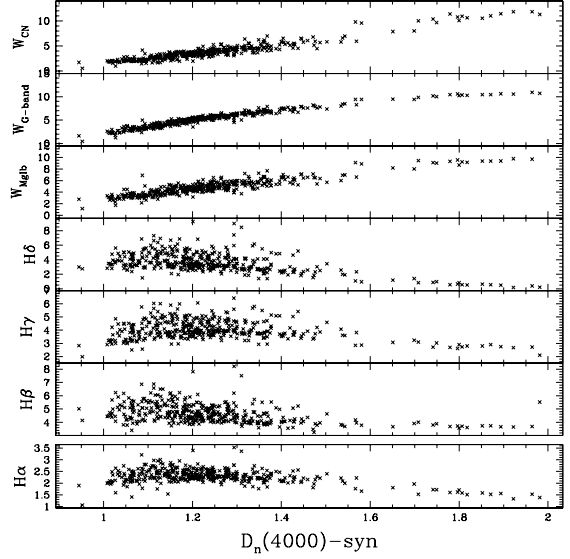


**Fig. 9.** Relations between  $D_n(4000)$  and equivalent widths of CN band, G band, Mg Ib,  $H\delta$ ,  $H\gamma$ ,  $H\beta$  and  $H\alpha$  measured in the synthetic spectrum. Correlations are clearly seen in almost all diagrams, however, the first three metal absorptions (top) show the strongest.

### 3.4. Stellar Features

We have measured a set of stellar indices directly from the synthetic spectra. For most of the stellar features, we use the same indices as defined by Cid Fernandes et al (2004a), which are based on the studies of star cluster and galaxy spectra by Bica & Alloin (1986a,b) and Bica (1988). We adopt the definition of Worthey & Ottaviani (1997) and Balogh et al (1999) for  $H\delta_A$  and  $D_n(4000)$  respectively. The results of the absorption lines are presented in Table 7: EWs of CaII K 3933 (Column 2), CN band 4200 (Column 3), G band 4300 (Column 4), Mg Ib 5173 (Column 5),  $H\delta$  4101 (Column 6),  $H\gamma$  4340 (Column 7),  $H\beta$  4861 (Column 8),  $H\alpha$  6563 (Column 9), and  $D_n(4000)$  (Column 10), all in units of  $\text{\AA}$ .

Kauffmann et al. (2003) have found that  $D_n(4000)$  is a useful indicator for stellar population during their study of SDSS galaxies, which has also been confirmed by the study of Seyfert 2 galaxies (Cid Fernandes et al 2004b). In Figure 9, we present the relations between  $D_n(4000)$  and model-derived equivalent widths of 3 absorption lines in the Bica's system: CN band, G band, Mg Ib and 3 Balmer absorption lines ( $H\beta$ ,  $H\gamma$  and  $H\delta$ ). The equivalent widths of CN band, G-band and Mg Ib are strongly correlate with  $D_n(4000)$ , and the three Balmer lines do exit correlation, although not very tight comparably.

One of the useful application of stellar population synthesis methods is to decompose the stellar contributions from the integrated spectrum to obtain pure nebular emission lines. Thus to derive accurate corrections of Balmer absorption features is particularly necessary. Previous study by McCall, Rybski & Shields (1985) re-



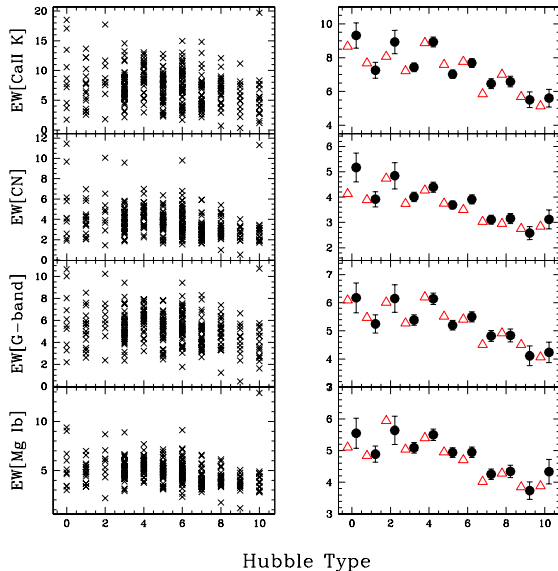


**Fig. 10.** Relations between Hubble types and equivalent widths of CaII K, CN band, G band and Mg Ib lines measured in the synthetic spectrum. There exist a decreasing trend from early-type spirals to the late-type, especially for those later than Sbc. Symbols are the same meaning as Figure 4

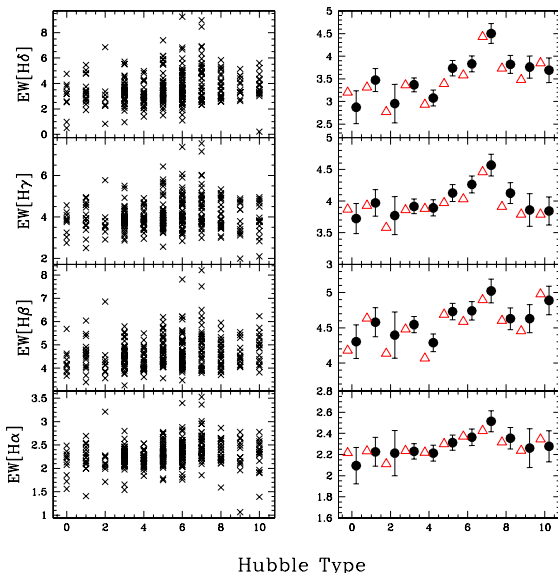


**Fig. 11.** Relations between Hubble types and equivalent widths H $\delta$ , H $\gamma$ , H $\beta$  and H $\alpha$  absorption lines measured in the synthetic spectrum. Interesting increasing EWs from Sbc to Sd type is found in all four measured Balmer absorption lines.

ommended a mean absorption correction of 2 Å to the EWs for the first three Balmer lines. Veilleux et al. (1995) also obtained a correction 2 Å for EW(H $\beta$ ) of the old stellar population, ranging from 1 to 3 Å. More recently, in the study of SFHs for a sample of starburst galaxies, Mayya

et al. (2004) got the mean absorption EWs of 1.57, 2.48, 2.32, 2.49 Å for the first four Balmer lines. In our studies, the mean average Balmer absorption EWs of H $\alpha$ , H $\beta$ , H $\gamma$  and H $\delta$  are 2.30, 4.68, 4.07 and 3.62, respectively.

Figure 10 and 11 show the distributions of 8 stellar absorption EWs: CaII K, CN band, G-band, Mg Ib, H $\alpha$ , H $\beta$ , H $\gamma$  and H $\delta$  along the Hubble types. The four metallic absorption features show a clear trend decreasing from the early-type spirals to late-type and irregular ones, especially for those later than Sbc. On the other hand, the four Balmer absorption lines exhibit an interesting increasing from Sbc to Sd type galaxies, though all these variations are actually small. Thus, the correction due to the Balmer absorption features should not be considered as a completely uniform value, but rather as a variation among the Hubble types.

#### 4. Bar Influence On the Star Forming Activity

Bar structures are well known to efficiently enhance the star formation activities of the circumnuclear regions (Huang et al. 1996, Ho et al. 1997b, Kennicutt 1998). Many numerical simulations have predict that a bar can effectively drive radial inflow of gas toward the center of a galaxy, which induce the burst of star formation (e.g., Roberts, Huntley & van Albada 1979; Elmegreen 1988; Athanassoula 1992; Piner, Stone & Teuben 1995).

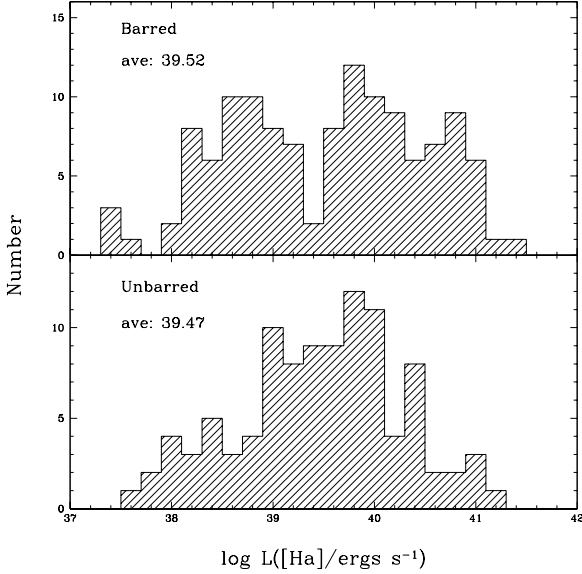
In all the 385 star forming galaxies, 157 are non-barred galaxies, 51 are weak barred galaxies (SAB), and 106 contain strong bars (SB), ranging from lenticular to irregular galaxies. Thus we get almost equal number of barred and unbarred galaxies in our sample (there are another 3 barred galaxies in the remaining 65 galaxies with uncertain morphologies, while the other 6 are elliptical galaxies). It is obvious that barred galaxies do show a quite common existence in every individual Hubble types.

The comparison between H $\alpha$  luminosities in barred and unbarred galaxies is shown in Figure 12. The barred galaxies show a large fraction toward the high end of L(H $\alpha$ ). Interesting gap between high and low part of luminosities does also exist in Fig. 3 of Ho et al. (1997b). Figure 13 shows the distribution of both the individual galaxies and the mean star formation rates of our sample, but this time separated into barred (filled circle) and unbarred (open triangle) types. It is clear that bars can enhance star formation, or at least extend the range toward the higher SFRs. This trend mainly occurs in the early-type spirals which is consistent with previous study of Huang et al. (1996) and Ho et al. (1997b).

Less agreement is found in the distribution of EW(H $\alpha$ )s (Figure 14). In general, the equivalent widths of H $\alpha$  of barred galaxies are higher than unbarred ones, but not significant in many individual types. We do find clear enhancement in EW(H $\alpha$ ) of barred galaxies (Figure 15), however, the largest difference is seen in the very late

**Table 3.** The bar existence among different morphological types

Galaxy Type	L	S0/a	Sa	Sab	Sb	Sbc	Sc	Scd	Sd	Sdm	Sm	Irr
Normal	22	3	11	4	16	15	19	23	18	13	2	11
SAB	3	0	1	1	6	7	13	8	4	5	1	2
SB	4	7	4	4	19	7	12	16	13	7	10	3

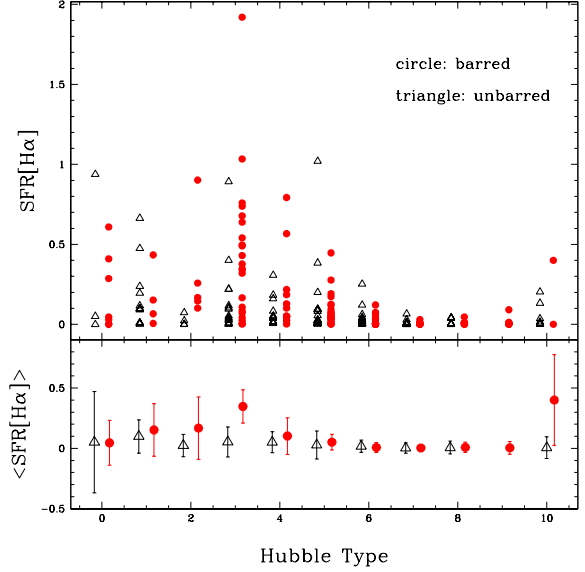
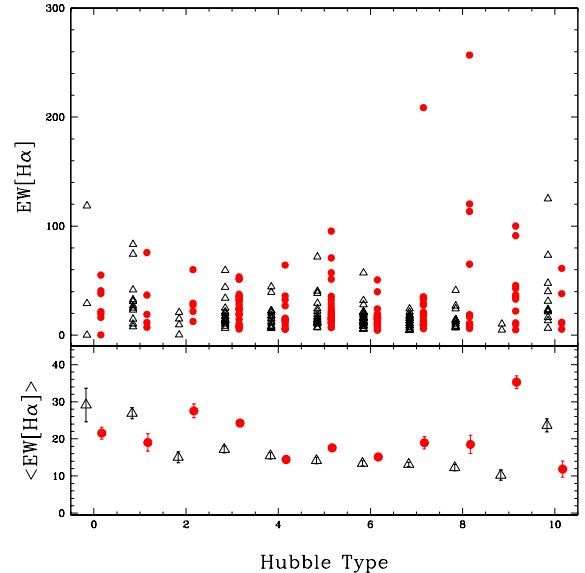
**Fig. 12.** Distribution of H $\alpha$  luminosities, extinction corrected. From top to bottom are barred and unbarred galaxies. Interesting gap between barred higher L(H $\alpha$ ) part and lower one of barred galaxies also exist in Fig. 3 of Ho et al. (1997b).

types. Since late-type spirals are believed to be gas rich, thus, other influence like gas contents and interactions may also play an important roll in the circumnuclear star formation activities.

## 5. Conclusions

We have constructed a sample of galaxies by positionally matching up the SDSS and RC3 data. We then applied the stellar population synthesis model to statistically study the variations of the star formation histories and line features along the Hubble types. Our finding are summarized as follows:

1. A decreasing sequence is found for nebular extinction from early-type spirals to late-type ones, which is consistent with previous studies of Ho et al. (1997a) and Stasińska et al. (2004). We have also confirmed that nebular emissions do suffer more serious extinctions than stellar light and the later one shows almost no variations among the Hubble types.
2. We find that H $\alpha$  luminosities of early-type spiral galaxies are much higher than the late-type ones, which causes the corresponding larger SFRs in early-type spirals. From the equivalent widths of H $\alpha$ , we find in gen-

**Fig. 13.** The SFRs of barred and unbarred galaxies as a function of Hubble T-type. From top to bottom are the distribution of individual galaxies and their average values. Filled circles represent the barred galaxies, while the open triangles show the unbarred ones. The errorbar is the deviation in the mean.**Fig. 14.** The EW[H $\alpha$ ] of barred and unbarred galaxies as a function of Hubble T-type. From top to bottom are the distribution of individual galaxies and their average values. Symbols are the same meaning as Figure 13



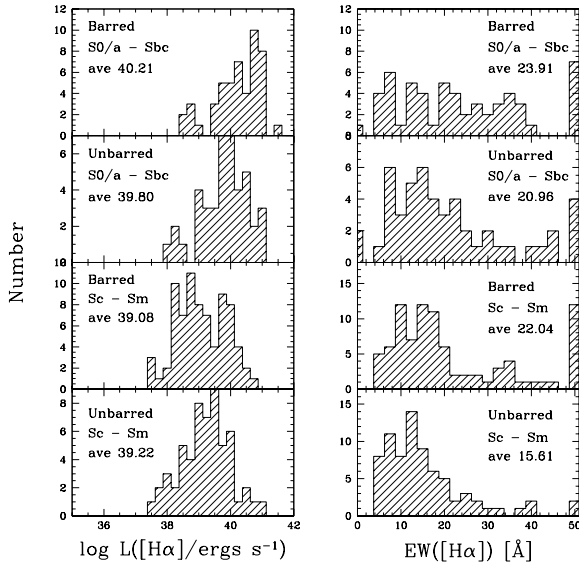


**Fig. 15.** The histograms of the extinction-corrected  $L[\text{H}\alpha]$  (left) and  $\text{EW}(\text{H}\alpha)$ s (right). The two top panels show the barred and unbarred galaxies in early-type spirals (S0/a-Sbc) and the two bottoms show the late-type spirals (Sc-Sm).

eral, early-type spirals show higher value of EWs, however, the dramatic change is found from Sdm type. We also plot the FIR-SFRs as a function of Hubble types and found that the early-type spirals show higher amount of FIR-SFRs and may partly due to the dust re-emission which will favor the early types. However, this difference of SFRs in IR band is comparably much smaller. Although large amount of galaxies show quite modest SFRs and may not actually contain bright HII regions, those who have strongly favor the higher star-forming activities in early-type galaxies.

3. We have measured the spectral absorption features and confirmed previous findings that tight correlations between  $D_n(4000)$  and equivalent widths of absorption lines: CN band, G-band, Mg Ib, H $\delta$ , H $\gamma$ , H $\beta$  and H $\alpha$ . The dependence of mean EWs on the Hubble types could be seen in metallic absorption lines. We also find an increase sequence of mean Balmer absorption equivalent widths from Sbc to Sd type. Since all these EWs are measured automatically, they do not depend on the morphology types.
4. We have discussed the bar effects on the star forming activities on both early-type and late-type spirals, and confirmed previous findings that bar structures can enhance the star forming activities, especially in early type spiral galaxies. However, bars are not necessarily inducing strong star formation activities; and those without could still contain high star formation regions. We also find that, though in general, the barred early-type spirals show larger  $\text{EW}[\text{H}\alpha]$ , the largest difference of  $\text{EW}[\text{H}\alpha]$  between barred and unbarred galaxies do

exist in the very late-type spirals (Sd  $\sim$  Sm). Thus we believe that other effects like interactions and gas contents may also play important roles in the star formation activities.

*Acknowledgements.* We would like to thank the anonymous referee for instructive comments which improved the content of the paper and thank Roberto Cid Fernandes for sending us the updated code for stellar population synthesis. This work is supported by the National Natural Science Foundation of China under grant 10221001 and the National Key Basic Research Science Foundation (NKBRSG19990754). Funding for the creation and distribution of the SDSS Archive has been provided by the Alfred P. Sloan Foundation, the Participating Institutions, the National Aeronautics and Space Administration, the National Science Foundation, the U.S. Department of Energy, the Japanese Monbukagakusho, and the Max Planck Society. The SDSS web site is <http://www.sdss.org/>. The SDSS is managed by the Astrophysical Research Consortium (ARC) for the Participating Institutions. The Participating Institutions are The University of Chicago, Fermilab, the Institute for Advanced Study, the Japan Participation Group, The Johns Hopkins University, Los Alamos National Laboratory, the Max-Planck-Institute for Astronomy (MPIA), the Max-Planck-Institute for Astrophysics (MPA), New Mexico State University, University of Pittsburgh, Princeton University, the United States Naval Observatory, and the University of Washington. This research has made use of the NASA/IPAC Extragalactic Database (NED) which is operated by the Jet Propulsion Laboratory, California Institute of Technology, under contract with the National Aeronautics and Space Administration.

## References

- Abazajian, K., et al. 2003, AJ, 126, 2081A  
 Abazajian, K., et al. 2004, AJ, 128, 502A  
 Athanassoula, E. 1992, MNRAS, 259, 345  
 Baldwin, J.A., Phillips, M.M., & Terlevich, R. 1981, PASP, 93, 5  
 Balogh, M., Morris, S., Yee, H., et al. 1999, ApJ, 527, 54  
 Bell, E.F., & Kennicutt, R.C. 2001, ApJ, 548, 681  
 Bica, E., Alloin, D. 1986a, A&A, 162, 21  
 Bica, E., Alloin, D. 1986b, A&A, 166, 83  
 Bica, E. 1988, A&A, 1995, 76  
 Blanton M. R. et al. 2005, AJ, 129, 2562  
 Bruzual, G., & Charlot, S. 2003, MNRAS, 344, 1000  
 Calzetti, D., Kinney, A.L., & Storchi-Bergmann, T. 1994, ApJ, 429, 582  
 Cardelli, J.A., Clayton, G.C., & Mathis, J.S. 1989, ApJ, 345, 245  
 Cid Fernandes, R., Sodre, L., Schmitt, H.R., et al. 2001, MNRAS, 325, 60  
 Cid Fernandes, R., Delgado, R.M.G., Schmitt, H.R., et al. 2004a, ApJ, 605, 105  
 Cid Fernandes, R., Gu Q., Melnick, J., et al. 2004b, MNRAS, 355, 273  
 Cid Fernandes, r., Mateus, A., Sodre, L., Stasinska, G., & Gomes, J.M. 2005, MNRAS, inpress (astro-ph/0412481)  
 Condon, J.J. 1992, ARA&A, 30, 575  
 Cram, L., Hopkins, A., Mobasher, B., & Rowan-Robinson, M. 1998, ApJ, 507, 155

- de Souza R. E., Gadotti D. A., dos Anjos S., 2004, ApJS, 153,411
- Deharveng, JM., Sasseen, TP., Buat, V., Bowyer, S., Lampton, M., Wu, X. 1994, A&A, 289, 715
- de Vaucouleurs, G., de Vaucouleurs, A., Corwin, H.G., Buta, R.J., Paturel, G., & Fouque, P. 1991, *Third Reference Catalogue of Bright Galaxies (New York: Springer) (RC3)*
- Devereux, NA. 1987, ApJ, 323, 91
- Devereux, NA., Becklin, EE., Scoville, N. 1987, ApJ, 312, 529
- Donas, J., Deharveng, JM. 1984, A&A, 140, 325
- Elmegreen, B.G. 1988, ApJ, 326, 616
- Giuricin, G., Tamburini, L., Mardirossian, F., Mezzetti, M., Monaco, P. 1994, A&A, 427, 202
- Gordon, K.D., Calzetti, D., & Witt, A.N. 1997, ApJ, 487, 625
- Hameed, S., Devereux, N. 2005, AJ, 129, 2597
- Harper, DA., Low F.J. 1973, ApJ Lett., 182, L89
- Hirashita H., & Ferrara A., 2002, MNRAS, 337, 921
- Ho, L.C., Filippenko, A.V., Sargent, W.L.W. 1997a, ApJ, 487, 579
- Ho, L.C., Filippenko, A.V., Sargent, W.L.W. 1997b, ApJ, 487, 591
- Huang, J.H., Gu, Q.S., Su, H.J., Hawarden, T.G., Liao, X.H., Wu, G.X. 1996, A&A, 313, 13
- Hubble, E. 1926, ApJ, 64, 321
- James, P.A., Shane, N. S., Beckman, J. E., Cardwell, A., et al. 2004, A&A, 414, 23
- Kauffmann, G., Heckman, T., White, S., et al. 2003, MNRAS, 341,33
- Keel, W.C. 1983, ApJ, 269, 466
- Kewley, L.J., Dopita, M.A., Sutherland, R.S., Heisler, C.A., Trevena, J. 2001, ApJ, 556, 121
- Kennicutt, R.C. 1983, ApJ, 272, 54
- Kennicutt, R.C., Kent, S.M. 1983, AJ, 88, 1094
- Kennicutt, R.C., Keel W.C., van der Hulst, J.M., Hummel, E., Roettiger, KA. 1987, AJ, 93, 1011
- Kennicutt, R.C., Keel, W.C., Blaha, C.A. 1989, AJ, 97, 1022
- Kennicutt, R.C., Tamblyn, P., Congdon, C.W. 1994, ApJ, 435, 22
- Kennicutt, R.C. 1998, ARA&A, 36, 189
- Lutz, D., Genzel, R., Sternberg, A., Netzer, H., Kunze, D., et al. 1996, A&A, 315, L137
- Madau, P., Pozzetti, L., Dickinson, M. 1998. ApJ, 498, 106M
- Mas-Hesse, J.M., & Kunth, D. 1999, A&AS, 349, 765
- Mayya, Y., Bressan, A., Rodríguez, M., Valdes, J.R., Chavez, M. 2004, ApJ, 600, 188
- McCall, M., Rybski, P., & Shields, G. 1985, ApJS, 57, 1
- Morgan, W.W. 1958, PASP, 70, 364
- Omukai, K. 2000, ApJ, 534, 809
- Osterbrock, D.E. 1989, *Astrophysics of Gaseous Nebulae and Active Galactic Nuclei (Mill Valley: University Science Books)*
- Piner, B.G., Stone, J.M., & Teuben, P.J. 1995, ApJ, 449, 508
- Rieke, G.H., Lebofsky, M.J. 1978, ApJ Lett.220, L37
- Roberts, W.W., Huntley, J.M., & van Albada, G.D. 1979, ApJ, 233, 67
- Schlegel, D.J., Finkbeiner, D.P., Davis, M. 1998, ApJ, 520, 525
- Scoville, N.Z., Becklin, E.E., Young, J.S., Capps, R.W. 1983, ApJ, 271, 512
- Sérsic, J.L., Pastoriza, M. 1967, PASP, 79, 152
- Stasińska, G., Mateus, A.Jr., Sodr , L.Jr., & Szczerba, R. 2004, A&A, 420, 475
- Stauffer, J.R. 1982, ApJS, 50, 517
- Stoughton, C., et al. 2002, AJ, 123, 485
- Telesco, C.M., Harper, D.A. 1980, ApJ235, 392
- Torres-Peimbert, S., Peimbert, M., Fierro, J. 1989, ApJ, 345, 186
- Veilleux, S., Kim, D-C., Sanders, D.B., Mazzarella, J.M., Soifer, B.T. 1995, ApJS, 98, 171
- Véron-Cetty, M.P., Véron, P. 2003, A&A, 412, 399V
- Worthey, G., Ottaviani, D.L. 1997, ApJS, 111, 377
- York, D.G., et al. 2000, AJ, 120, 1579
- Young, J.S., Allen, L., Kenney, J.D.P., Lesser, A., Rownd, B. 1996, AJ, 112, 1903

**Table 4.** Catalog of the whole sample

Name	R.A.(2000)	Dec.(2000)	Redshift	$A_{v_{st}}$	$A_{v_{neb}}$	$\log L_{FIR}^a$	Morphology
NGC3042	09h53m20.2s	+00d41m51.8s	0.012613	0.1073	---	--	S0
UGC5238	09h46m53.5s	+00d30m26.4s	0.005929	0.7515	0.7775	--	SBdm
UGC7963	12h47m52.9s	-01d11m08.9s	0.023371	0.9519	---	--	Sdm
A1252+00	12h55m12.6s	+00d06m59.9s	0.004180	0.0295	0.5290	--	SBd
NGC4668	12h45m31.9s	-00d32m08.5s	0.005431	0.1912	0.3029	42.38	SBd
CGCG15-20	12h47m19.3s	+00d24m17.4s	0.047169	-0.0587	---	--	S0
MCG0-29-27	11h24m08.6s	-01d09m27.9s	0.029288	0.5686	1.0296	--	SAB0
UGC6435	11h25m35.0s	-00d46m05.6s	0.025325	-0.0924	---	--	S0
UGC6340	11h19m55.4s	-00d52m47.9s	0.024573	-0.0535	---	43.65	SABbc
UGC6432	11h25m17.9s	+00d21m01.8s	0.040292	0.2952	0.2812	--	SAbc
CGCG11-100	11h27m36.7s	+00d23m42.8s	0.049075	0.3285	---	--	SBb
MCG0-29-29	11h24m18.6s	+00d38m37.4s	0.026402	0.2049	1.3175	--	SBc
UGC9299	14h29m34.6s	-00d01m05.7s	0.005204	0.2909	-0.1752	--	SABd
IC1010	14h27m20.3s	+01d01m33.2s	0.025687	0.2471	---	--	SBb
MCG0-29-36	11h28m16.4s	+00d53m28.9s	0.039884	0.2740	0.7626	--	SABbc
UGC6402	11h23m19.1s	-00d55m21.4s	0.008698	0.9888	1.3155	43.04	Sdm
UGC6457	11h27m12.2s	-00d59m40.8s	0.003191	0.5764	-0.0508	--	dIn
MCG0-30-4	11h31m58.6s	-00d03m01.1s	0.039859	0.7349	---	--	SACd
MCG0-29-28	11h24m09.1s	+00d42m01.9s	0.025987	0.4158	0.0219	--	Sc
NGC3719	11h32m13.4s	+00d49m09.3s	0.019457	0.1252	0.3016	--	SAbc
CGCG11-103	11h27m57.5s	-01d12m40.1s	0.042687	1.5888	1.9545	--	SA0
IC992	14h18m14.9s	+00d53m28.0s	0.025965	0.3778	1.1523	43.75	SABc
UGC5195	09h43m12.0s	+00d24m51.0s	0.025190	0.8237	0.9703	43.74	Sbc
UGC5205	09h44m07.2s	-00d39m29.7s	0.005003	-1.6866	---	--	SBm
UGC5242	09h47m05.5s	+00d57m51.9s	0.006137	-0.1979	0.0223	--	SBm
IC1011	14h28m04.5s	+01d00m22.8s	0.025647	0.3966	0.6289	43.68	—
UGC6608	11h38m33.2s	-01d11m04.2s	0.020776	0.8511	1.4847	43.52	SABab
MCG0-30-7	11h32m45.4s	-00d44m27.7s	0.022379	0.4967	0.2987	--	SBm
CGCG12-54	11h40m06.4s	-00d50m15.7s	0.019591	-0.1357	---	--	E
CGCG12-27	11h34m39.1s	+00d07m29.1s	0.028791	0.2434	---	--	SA0/a
CGCG12-5	11h32m09.2s	-00d56m33.4s	0.026154	-0.0494	---	--	SAB0
CGCG12-53	11h40m06.2s	-00d54m05.0s	0.028712	0.6698	1.5266	--	SAb
IC716	11h39m03.3s	-00d12m21.6s	0.018078	0.6377	---	--	Sbc
NGC3720	11h32m21.8s	+00d48m17.0s	0.020068	0.1563	0.9369	44.09	SAa
NGC5750	14h46m11.1s	-00d13m22.6s	0.005827	0.3941	---	42.52	SB0/a
NGC5733	14h42m45.9s	-00d21m03.8s	0.005698	0.4660	0.0989	--	dIn
UGC9470	14h41m48.6s	+00d41m13.1s	0.006427	1.3992	---	--	SBdm
UGC9977	15h41m59.5s	+00d42m46.0s	0.006483	1.3629	0.1903	42.41	Sc
MCG0-39-4	15h07m59.2s	+01d13m54.2s	0.035114	0.5962	1.5006	44.05	S?
UGC9732	15h08m09.7s	+01d14m57.6s	0.035335	0.4407	0.7379	--	SBb
CGCG17-54	13h39m13.2s	-01d07m15.4s	0.014852	0.2651	0.3066	--	Sb
CGCG17-43	13h38m06.4s	+00d01m13.7s	0.022360	-0.1490	0.2262	--	HII?
NGC5887	15h14m43.9s	+01d09m15.4s	0.029286	0.1289	---	--	SA0
UGC10264	16h12m56.8s	-00d05m46.5s	0.030845	0.6339	---	43.88	SABcd
MCG0-41-5	16h10m14.6s	+01d03m20.5s	0.027844	0.6427	---	--	SABdm
IC4229	13h22m26.1s	-02d25m05.7s	0.023181	0.2678	0.9835	43.83	SBb
UGC10005	15h45m14.3s	+00d46m19.9s	0.012830	0.3854	---	--	SAd
A1301-03	13h04m31.1s	-03d34m20.6s	0.004623	-0.2095	0.1498	--	SABdm
UGC10306	16h16m43.5s	+00d14m47.2s	0.030720	0.0906	---	--	SABb
MK502	16h53m42.9s	+64d05m06.8s	0.041539	0.1778	---	--	Compact
IC1235	16h52m03.6s	+63d06m56.8s	0.010433	0.1460	0.0481	--	—
IC1248	17h11m40.1s	+59d59m44.2s	0.016699	0.3598	0.7844	--	SBc

<sup>a</sup> Luminosity in unit of  $\text{erg s}^{-1}$

**Table 5.** Flux densities of emissions

Name	F4861	F5007	F6548	F6584	F6563	F6717	F6731
NGC3042	87.60	206.83	215.99	715.24	356.47	173.07	174.66
UGC5238	221.14	343.76	50.40	131.92	839.97	136.81	100.51
UGC7963	40.52	16.64	25.60	68.87	169.61	35.46	25.17
A1252+00	117.13	69.67	61.47	133.81	406.33	106.49	75.72
NGC4668	77.33	111.44	25.37	62.83	247.01	50.40	40.74
CGCG15-20	32.83	63.76	41.08	100.76	85.81	33.22	37.83
MCG0-29-27	454.87	3623.94	474.27	1397.25	1894.18	476.63	436.90
UGC6435	32.27	54.61	54.48	143.85	100.85	45.46	63.48
UGC6340	59.64	113.27	52.29	133.68	159.19	93.57	83.84
UGC6432	67.03	40.45	27.58	69.79	212.42	29.59	23.91
CGCG11-100	84.60	59.61	48.37	170.48	382.18	53.53	41.48
MCG0-29-29	205.59	60.20	100.57	340.95	950.97	155.27	115.74
UGC9299	100.17	142.39	19.46	49.81	268.74	60.93	41.82
IC1010	28.23	50.21	37.40	114.03	77.11	40.71	45.17
MCG0-29-36	118.48	100.65	71.61	169.99	447.58	43.43	33.22
UGC6402	262.24	321.97	90.41	255.23	1212.12	240.04	170.32
UGC6457	74.76	119.94	6.10	19.30	209.89	47.78	35.90
MCG0-30-4	24.88	10.97	7.94	23.57	53.15	7.72	7.94
MCG0-29-28	85.01	26.07	32.01	90.03	245.07	40.70	28.08
NGC3719	99.62	73.50	69.68	206.05	318.08	79.54	64.01
CGCG11-103	176.13	597.52	371.61	1052.18	1027.92	186.33	192.54
IC992	413.55	149.43	239.34	733.45	1800.94	195.61	155.79
UGC5195	75.89	50.32	56.59	174.65	309.25	65.11	45.78
UGC5205	0.88	4.33	3.68	11.91	8.45	1.88	3.18
UGC5242	73.65	142.13	11.32	21.61	212.37	33.74	24.61
IC1011	264.94	116.42	133.05	427.08	953.21	174.78	131.63
UGC6608	144.86	51.48	115.72	339.64	712.22	116.92	101.07
MCG0-30-7	41.99	31.64	12.77	30.72	133.92	42.33	27.34
CGCG12-54	13.71	58.07	24.72	43.51	43.81	4.70	19.61
CGCG12-27	14.47	11.71	8.74	15.70	20.60	7.53	3.79
CGCG12-5	65.53	184.96	126.14	266.62	220.74	91.16	82.65
CGCG12-53	198.49	40.59	113.06	327.10	990.92	123.50	93.72
IC716	47.00	57.84	32.01	169.37	159.05	64.46	63.97
NGC3720	180.55	38.49	78.30	233.36	726.85	66.07	53.76
NGC5750	216.90	331.13	306.15	869.79	802.45	525.02	399.84
NGC5733	223.31	505.47	27.75	83.83	662.12	132.27	88.91
UGC9470	17.79	24.47	12.69	12.06	52.33	14.95	12.16
UGC9977	51.81	29.84	16.95	49.62	158.83	48.37	33.27
MCG0-39-4	855.21	292.04	764.47	2451.81	4229.11	752.21	658.27
UGC9732	81.72	90.88	98.14	250.93	305.94	108.88	77.93
CGCG17-54	78.90	28.70	24.87	86.00	252.37	57.94	38.02
CGCG17-43	153.46	136.86	38.97	125.39	476.67	110.59	79.35
NGC5887	64.82	110.90	122.43	299.64	182.45	124.74	108.50
UGC10264	30.11	87.02	22.06	77.12	94.72	32.00	21.27
MCG0-41-5	20.38	31.95	14.14	34.65	32.84	13.35	14.66
IC4229	1039.08	189.08	562.62	1755.09	4254.76	538.92	442.83
UGC10005	27.08	11.16	9.99	22.88	52.19	15.34	12.29
A1301-03	296.09	671.88	30.27	93.71	894.39	130.47	91.69
UGC10306	51.46	92.14	89.49	254.92	173.67	103.60	83.59
MK502	23.63	13.44	11.75	32.05	51.36	10.20	7.92
IC1235	233.19	210.91	60.58	170.31	678.74	180.12	126.67
IC1248	176.12	43.94	68.81	216.49	670.64	115.54	76.33

Flux densities are in units of  $10^{-17} \times \text{erg s}^{-1} \text{cm}^{-2} \text{\AA}$ .

**Table 6.** Equivalent widths of Emissions

Name	EW4861	EW5007	EW6548	EW6584	EW6563	EW6717	EW6731
NGC3042	0.31	0.67	0.71	2.33	1.17	0.52	0.53
UGC5238	34.32	43.76	7.29	18.64	120.30	21.19	15.58
UGC7963	3.52	1.30	2.14	5.69	14.12	2.54	1.80
A1252+00	3.73	1.91	1.87	3.99	12.25	4.05	2.89
NGC4668	3.18	3.90	0.94	2.32	9.14	2.24	1.81
CGCG15-20	0.50	0.92	0.64	1.56	1.33	0.47	0.54
MCG0-29-27	6.72	45.88	6.41	18.07	25.12	7.14	6.55
UGC6435	0.17	0.26	0.28	0.75	0.52	0.22	0.31
UGC6340	0.39	0.70	0.33	0.86	1.02	0.58	0.52
UGC6432	2.54	1.34	0.96	2.37	7.32	1.08	0.87
CGCG11-100	1.92	1.29	1.04	3.66	8.22	1.20	0.93
MCG0-29-29	6.48	1.77	3.02	10.27	28.62	6.24	4.66
UGC9299	8.85	9.53	1.41	3.57	19.39	5.66	3.89
IC1010	0.54	0.93	0.69	2.11	1.42	0.69	0.77
MCG0-29-36	3.17	2.50	1.82	4.27	11.31	1.20	0.92
UGC6402	10.34	10.50	3.10	8.52	41.06	9.12	6.47
UGC6457	6.87	11.27	0.59	1.87	20.27	6.77	5.09
MCG0-30-4	3.84	1.51	1.10	3.23	7.32	1.11	1.14
MCG0-29-28	4.34	1.16	1.51	4.14	11.41	2.00	1.38
NGC3719	2.36	1.65	1.61	4.74	7.33	1.89	1.52
CGCG11-103	6.78	18.08	10.40	29.90	28.96	4.02	4.15
IC992	12.18	4.12	6.86	20.75	51.35	6.75	5.38
UGC5195	3.03	1.73	2.04	6.38	11.19	2.08	1.46
UGC5205	0.12	0.43	0.41	1.40	0.97	0.36	0.62
UGC5242	15.28	27.75	2.50	4.46	45.58	9.73	7.11
IC1011	5.85	2.30	2.71	8.80	19.53	4.01	3.02
UGC6608	4.85	1.58	3.56	10.33	21.78	3.25	2.81
MCG0-30-7	7.33	5.35	2.14	4.95	22.07	8.23	5.32
CGCG12-54	0.16	0.68	0.30	0.53	0.53	0.05	0.23
CGCG12-27	1.37	1.00	0.76	1.36	1.80	0.65	0.33
CGCG12-5	0.72	1.87	1.39	2.89	2.41	0.95	0.87
CGCG12-53	8.12	1.36	3.89	11.10	33.90	4.49	3.41
IC716	0.76	0.86	0.47	2.58	2.38	0.82	0.81
NGC3720	6.26	1.18	2.49	7.38	23.08	2.70	2.20
NGC5750	1.21	1.68	1.62	4.59	4.24	2.59	1.98
NGC5733	7.76	16.69	0.95	2.85	22.59	6.07	4.09
UGC9470	3.04	4.15	2.07	1.91	8.42	2.89	2.35
UGC9977	4.18	2.33	1.25	3.75	11.81	3.26	2.24
MCG0-39-4	11.36	3.61	9.36	30.28	51.96	9.85	8.62
UGC9732	1.41	1.38	1.60	4.11	5.00	1.60	1.14
CGCG17-54	5.97	1.78	1.69	5.95	17.28	5.03	3.30
CGCG17-43	10.58	7.40	2.15	6.93	26.32	8.33	5.99
NGC5887	0.48	0.71	0.84	2.04	1.25	0.77	0.67
UGC10264	0.75	2.07	0.51	1.80	2.21	0.67	0.45
MCG0-41-5	0.69	1.01	0.46	1.13	1.07	0.36	0.40
IC4229	7.02	1.22	3.65	11.39	27.59	4.24	3.49
UGC10005	2.90	0.98	0.93	2.08	4.80	1.62	1.30
A1301-03	43.31	77.93	3.82	11.99	113.47	27.64	19.48
UGC10306	0.53	0.87	0.90	2.54	1.74	0.95	0.77
MK502	1.15	0.58	0.52	1.42	2.28	0.47	0.36
IC1235	5.92	4.50	1.34	3.76	14.99	5.41	3.81
IC1248	5.88	1.31	2.15	6.78	20.99	4.20	2.78

All equivalent wavelengths are in units of Å.

**Table 7.** Equivalent widths of absorptions

Name	EW3933	EW4200	EW4340	EW5173	EW4101	EW4300	EW4861	EW6563	$D_n(4000)$
NGC3042	17.63	11.38	10.38	9.19	0.70	2.96	3.84	1.64	1.83
UGC5238	5.66	2.59	4.41	3.81	3.06	3.49	3.94	2.23	1.15
UGC7963	8.56	4.73	6.29	5.95	2.92	3.84	4.13	2.11	1.29
A1252+00	7.50	3.24	5.42	4.71	4.07	4.43	4.78	2.35	1.20
NGC4668	7.93	3.26	5.36	4.58	3.40	3.98	4.59	2.41	1.22
CGCG15-20	17.81	10.89	10.41	9.36	0.59	2.96	3.72	1.49	1.87
MCG0-29-27	9.33	4.63	6.46	5.86	2.47	3.57	3.95	2.10	1.29
UGC6435	18.47	11.45	10.59	9.27	0.39	2.77	3.57	1.49	1.91
UGC6340	18.07	10.64	10.18	8.41	0.55	2.90	3.42	1.51	1.86
UGC6432	9.82	5.16	6.77	6.58	2.65	3.75	4.36	2.12	1.31
CGCG11-100	9.62	4.82	6.63	6.14	2.81	3.82	4.29	2.09	1.33
MCG0-29-29	2.82	1.84	3.38	3.31	4.81	4.05	4.71	1.75	1.12
UGC9299	4.14	2.23	3.99	3.69	5.54	5.03	5.40	2.63	1.14
IC1010	17.61	9.42	10.16	8.52	1.02	3.08	3.62	1.79	1.79
MCG0-29-36	11.26	5.45	7.02	6.37	2.54	3.70	4.44	2.23	1.37
UGC6402	2.90	2.05	3.31	3.43	5.84	5.15	5.67	2.64	1.13
UGC6457	2.11	1.81	2.22	2.62	3.61	3.35	4.87	2.27	1.02
MCG0-30-4	6.21	3.39	5.31	4.75	6.15	5.71	5.68	2.68	1.29
MCG0-29-28	9.49	4.27	6.35	5.48	3.32	4.09	4.40	2.30	1.31
NGC3719	13.46	6.50	8.46	7.39	1.52	3.12	3.61	1.89	1.48
CGCG11-103	13.39	6.54	7.12	5.10	3.74	4.32	4.79	0.90	1.57
IC992	5.67	3.18	4.50	4.55	3.51	3.84	4.73	2.29	1.14
UGC5195	12.53	5.44	7.52	5.99	3.00	4.17	4.29	2.29	1.48
UGC5205	8.57	4.92	6.47	7.45	2.61	3.40	5.07	1.70	1.21
UGC5242	5.82	2.21	4.53	3.77	5.14	4.89	5.54	2.78	1.16
IC1011	7.54	4.16	5.39	5.36	3.22	3.87	4.71	2.27	1.22
UGC6608	10.75	5.37	7.11	6.21	2.24	3.50	3.82	2.11	1.37
MCG0-30-7	6.50	3.34	4.58	4.07	4.62	4.66	5.30	2.66	1.20
CGCG12-54	17.88	11.54	10.65	9.74	0.62	2.73	3.86	1.61	1.84
CGCG12-27	14.44	6.79	8.44	7.12	2.02	3.67	3.98	2.13	1.55
CGCG12-5	18.00	10.54	10.54	9.41	0.57	2.82	3.62	1.55	1.84
CGCG12-53	7.22	4.08	5.21	4.89	3.39	4.00	4.53	2.32	1.21
IC716	17.04	9.28	9.89	8.15	1.24	3.33	3.69	1.88	1.77
NGC3720	4.97	3.47	4.25	5.10	2.86	3.38	4.66	2.09	1.09
NGC5750	14.87	8.14	8.75	7.64	1.94	3.78	4.21	2.05	1.60
NGC5733	3.82	2.29	3.31	3.32	3.85	3.84	4.86	2.42	1.08
UGC9470	0.70	0.98	1.24	1.74	3.78	3.00	4.08	1.59	1.03
UGC9977	4.89	3.35	4.95	4.35	7.40	6.43	6.19	2.78	1.29
MCG0-39-4	7.53	4.29	5.67	5.64	2.98	3.79	4.30	2.09	1.23
UGC9732	14.45	8.17	8.85	7.79	1.73	3.56	4.04	1.87	1.59
CGCG17-54	5.70	2.74	4.32	4.16	2.77	3.31	4.18	2.24	1.11
CGCG17-43	7.81	2.90	5.51	4.46	4.54	4.65	4.99	2.55	1.24
NGC5887	18.58	11.54	10.71	9.12	0.47	2.85	3.52	1.55	1.92
UGC10264	12.99	7.25	8.25	7.33	1.77	3.43	3.93	1.97	1.49
MCG0-41-5	15.59	8.53	9.55	8.05	1.27	3.26	3.64	1.84	1.66
IC4229	5.97	3.71	4.83	5.30	3.06	3.59	4.54	2.07	1.15
UGC10005	8.13	3.49	5.53	4.69	3.39	3.98	4.44	2.38	1.24
A1301-03	3.64	2.40	3.30	3.62	3.84	3.91	5.22	2.25	1.04
UGC10306	16.54	10.89	10.14	9.25	0.57	2.80	3.67	1.55	1.74
MK502	13.18	5.91	8.07	6.93	1.79	3.29	3.71	2.04	1.46
IC1235	4.98	2.71	4.31	3.98	5.36	5.00	5.69	2.64	1.15
IC1248	6.79	3.73	5.02	5.01	2.85	3.48	4.39	2.22	1.17

All equivalent wavelengths are in units of Å.



